ISSN 1075-7015, Geology of Ore Deposits, 2018, Vol. 60, No. 8, pp. 708–716. © Pleiades Publishing, Ltd., 2018.
Original Russian Text © A.I. Gusev, 2017, published in Zapiski Rossiiskogo Mineralogicheskogo Obshchestva, 2017, No. 4, pp. 54–64.

MINERALS AND MINERAL ASSEMBLAGES

Composition of Magmatic and Hydrothermal Zircon in the Elinovskii Massif, Gorny Altai

A. I. Gusev*

Shukshin Altai State Humanities Pedagogical University, Biisk, 659333 Russia

**e-mail: anzerg@mail.ru*

Received November 23, 2016

Abstract—The paper discusses new SHRIMP II data on the absolute age of riebeckite granite of the Elinovskii massif, Gorny Altai, and presents comparative characteristics of the morphology and chemical composition of magmatic and hydrothermal zircon obtained by LA-ICP-MS. It is shown that the revealed differences between the two types of zircon are related to the peculiarities of the fluid regime of granitoid melts. Both types of zircon manifest the tetrad effect of M-type REE fractionation.

Keywords: riebeckite granite, leucogranite, U–Pb age, zircon, rare-earth elements, REE fractionation, Gorny Altai

DOI: 10.1134/S1075701518080044

INTRODUCTION

Zr and other incompatible elements, such as REE, Nb, Y, Be, Th, and U, can be highly mobile in alkaline and fluorine-enriched felsic melts (Bau, Dulski, 1995; Aja et al., 1997; Veksler et al., 2005; Ayers et al., 2012). Experimental studies show that the coefficients of REE and Y distribution between a fluorine-enriched aqueous fluid and silicate melt vary from 100 to 200 (Veksler et al., 2005). Examples are fluids of the Strange Lake pluton in Canada (Salvi and Williams-Jones, 2006) and the Berzhei pluton in China (Jahn et al., 2001). In the rocks of these intrusions, zircon plays an important role in the concentration of these elements. High field strength elements have high charge-to-ion-radius ratios; therefore, they are incompatible in magmatic fractionation processes (Finlowbates and Stumpil, 1981). Experimental studies have shown that in certain cases these elements are mobile and are concentrated during the fractional crystallization of granite and pegmatite melts (Salvi and Williams-Jones, 2006; Van Lichtervelde et al., 2010). Zircon can have both magmatic and hydrothermal origins (Hoskin and Schaltegger, 2003; Pettke et al., 2005; Belousova et al., 2006). Zircon varieties differ in the zoning, morphology, and geochemistry of REE (Rubin et al., 1989; Sinha et al., 1992; Hoskin, 2005; Pettke et al., 2005; Schaltegger et al., 2005; Schaltegger, 2007; Gasquet et al., 2007; Lawrie et al., 2007; Fu et al., 2009). Hydrothermal zircon can precipitate out of fluid-saturated magmas (Schaltegger, 2007) and carry information on the peculiarities of hydrothermal events (McNaughton et al., 2005; Gasquet et al., 2007; Valley et al., 2009, 2010; Van Lichtervelde et al., 2009). The genetic relationship between magmatic and hydrothermal zircon from granite plutons may reveal the evolution from magmatic to hydrothermal processes in the formation of rare metal deposits (Pettke et al., 2005; Schaltegger et al., 2005).

ANALYTICAL RESEARCH METHODS

Local U–Pb analysis of zircon for absolute age determination was performed on a SHRIMP II secondary ion mass spectrometer (SIMS) at the VSEGEI Center of Isotopic Research. The U–Pb ratios were normalized to a value of 0.0668 assigned to the TEMORA standard zircon. The errors in measuring single analyses are given for the interval of 1σ, and the errors of calculated concordant ages and intersections with concordia, at a level of 2σ. The U–Pb age was calculated with the ISOPLOT/EX program.

The trace element composition of zircon was studied by LA-ICP-MS with a Finnigan Mat ELEMENT mass spectrometer combined with a New Wave Research UP-213, Nd:YAG laser attachment. The main elements were determined on a JEOL JXA-8100 wave microprobe (at the Analytical Center of the Institute of Geology and Mineralogy, Siberian Branch, Russian Academy of Sciences).

The tetrad effect of REE fractionation was calculated with B. Irber's formula (Irber, 1999).

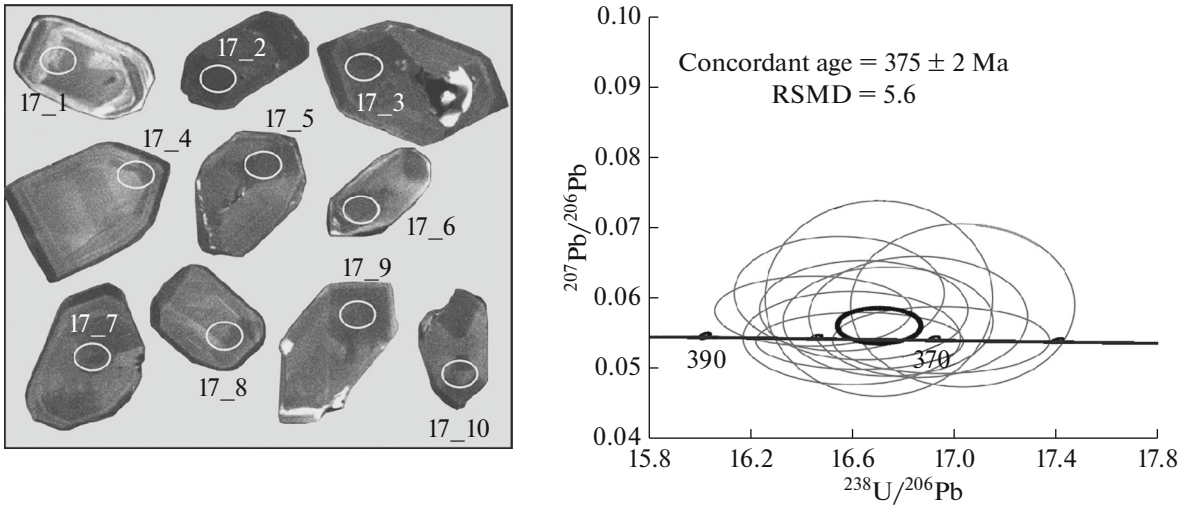

Fig. 1. Morphology of zonal zircon crystals and U-Pb plot with concordia for zircon from riebeckite granite of the Elinovskii massif.

GEOLOGICAL DESCRIPTION

The Elinovskii granitoid massif is located in the left wall of the Shchebet River Valley (a left tributary of the Anui River) and is a northeast-trending fracture body more than 2 km in extent and from 0.5 to 1 km wide. At the northeast continuation of the massif, several dikes are observed extending from 0.5 to 1 km and measuring from 0.3 to 50 m in thickness. The massif consists of riebeckite granite and leucogranite with rosy and yellow-gray hues. Prismatic feldspar (50–60%) and quartz (up to 30–35%) predominate among leucogranites in the massif. The characteristic dark-colored mineral is amphibole, which is nonuniformly distributed in rock and forms rare glomeroporphyritic segregations. Its content varies from 3 to 6%, 4% on average. Astrophyllite and aegirine are encountered sporadically. Rocks have a characteristic hypidiomorphic texture, which locally transitions to xenomorphic-granular. Amphibole is represented by large (up to 0.5–1 cm) elongate prismatic crystals nearly black in color with a brownish blue hue. Recalculation to the structural formula for the chemical composition of amphibole shows that, in the degree of sodium filling of positions *A* and *B* ($Na_A + Na_B = 2.11–2.15$), it is close to riebeckite (for riebeckite $Na_A + Na_B = 2$, and for arfvedsonite, $Na_A + Na_B = 3$). In addition, the closeness to riebeckite is also established by the absence of aluminum in the octahedral coordination (Al_{VI}). Microperthite feldspar forms prismatic crystals in granite. It is characterized by almost equal amounts of sodium and potassium with a certain predominance of the latter.

At the contact with the massif is the Elinovskii fluorite–REE occurrence, located at the watershed of the Bablaiki and Shchebety rivers (Gusev and Tabakaeva, 2015). It was discovered by A.V. Krivchikov in 1957. In 1958, 14 trenches were dug, exposing the mineralization. The ore zone is associated with the contact of medium-grained riebeckite granite of the Elinovskii massif with limestone of the Upper Silurian Kuimov Formation. Granite near the contact has been albitized, kaolinized, silicified, and ocherized via fractures. K-feldspar with quartz veinlets and impregnations of fluorite, zircon, monazite, xenotime, synchysite, and columbite have been observed locally. The contents of elements in albititzed granite vary (wt %): zircon, from 0.1 to 1.2; yttrium, from 0.2 to 0.7; ytterbium, from 0.1 to 0.5; niobium, from 0.05 to 0.3). REE are included in the chemical composition of polycrase, monazite, xenotime, fergusonite, and zircon, which are localized in albitized granite and fluorite–quartz veins. The sizes of zircon crystals are 0.1–0.2 mm. Albitized granite manifests pitchblende mineralization with a uranium content of 0.1–1.5 wt %.

MORPHOLOGY AND CHEMICAL COMPOSITION OF ZIRCON

In alkaline granite of the Elinovskii massif, zircon is equant, frequently pancake-shaped, rarely (20% of crystals) subeuhedral, and sporadically euhedral. The mineral is yellowish, rosy, and up to reddish brown in color. Zircon contains many numerous inclusions and possesses coarse zoning. The outer corona is dark. Ten measurements yielded an age of 369 ± 10 Ma (Late Devonian) (Fig. 1). The uranium and thorium contents are 456–1102 and 180–639 ppm, respectively; Th/U = 0.31–0.60.

In magmatic zircon, the {100} faces are more frequently developed and {110} faces of the prism are absent, which indicates that zircon crystallized from a high-temperature melt (Pupin, Turco, 1972).

In contrast to the magmatic variety, hydrothermal zircon has a bipyramidal habit with well-developed {111} faces, and it is close in morphology to synthetic

Table 1. Chemical composition of magmatic zircon from the Elinovskii massif (oxides in wt %, trace elements in ppm)

Component	1	2	3	4	5	6	7	8	9	10
SiO_2	33.4	33.5	33.1	33.4	33.4	33.5	33.4	33.3	33.3	33.4
ZrO_2	66.3	66.2	66.4	66.2	66.1	66.0	66.2	66.2	66.1	66.2
P_2O_5	0.036	0.033	0.034	0.06	0.037	0.03	0.04	0.039	0.032	0.064
Sc	105	103	91	95	105	102	99	97	99	96
Ti	2.5	2.6	2.3	3.1	4.2	3.3	2.9	3.0	3.2	3.5
Y	505	438	446	494	493	566	553	592	570	495
Nb	2.51	2.62	2.42	1.99	2.61	2.59	2.85	3.5	2.97	1.99
La	0.2	0.61	0.9	0.58	0.49	0.47	0.23	0.65	0.23	0.4
Ce	41.5	34.8	40.7	32.7	39.8	34.8	36.9	48.5	39.9	33.8
Pr	0.066	0.051	0.063	0.12	0.094	0.047	0.11	0.074	0.062	0.1
Nd	1.5	0.89	1.49	1.07	1.09	1.32	1.27	1.44	1.14	1.07
Sm	2.04	1.63	1.95	1.57	2.09	2.04	1.6	2.1	2.11	1.57
Eu	0.68	0.65	0.61	0.59	0.72	0.56	0.73	1.01	0.7	0.62
Gd	10.4	8.5	9.4	8.4	10.1	10.7	10.9	11.1	10.9	8.4
Tb	3.16	2.58	2.75	2.58	2.91	3.13	3.28	3.6	3.22	2.58
Dy	40.7	42.6	46.2	38.5	38.4	43.7	43.9	45.5	44.2	42.0
Ho	15.5	12.1	13.1	11.4	13.6	15.3	15.0	16.4	14.8	13.4
Er	81.9	72.1	78.2	72.1	73.8	87.8	87.6	93.3	89.1	72.1
Tm	19.8	16.1	17.2	17.1	19.3	23.9	22.5	22.9	24.1	18.1
Yb	199	164	173	174	189	241	238	237	229	194
Lu	43.8	32.1	34.6	32.1	41.3	51.3	48.6	51	49.8	32.1
Hf	9850	9870	9910	9860	9940	9990	9512	9955	9950	9960
Ta	0.88	0.72	0.78	0.72	0.87	0.96	1.03	1.05	0.95	0.71
Pb	9.0	7.9	9.7	7.9	10.6	6.6	9.21	11.6	8.4	7.7
Th	180	556	639	199	241	192	198	247	199	188
U	456	1100	1102	916	876	778	905	989	990	655
ΣREE	965.2	826.7	866.2	886.8	925.7	1082.1	1063.6	1126.6	1079.3	915.2
Th/U	0.39	0.5	0.58	0.21	0.28	0.25	0.22	0.25	0.2	0.29
$(La/Yb)_N$	0.001	0.002	0.003	0.002	0.002	0.001	0.001	0.002	0.001	0.002
Eu/Eu*	0.37	0.44	0.36	0.4	0.39	0.3	0.4	0.52	0.37	0.42
Ce/Ce*	87.9	28.3	29.6	28.4	41.6	45.8	54.2	44.7	79.4	46.8
Y/Ho	32.6	36.2	34.0	43.3	36.3	37.0	36.9	36.1	38.5	36.9
$TE_{1.3}$	2.62	1.84	1.53	2.31	2.3	1.6	3.11	1.84	2.13	2.36

In Tables 1 and 2, the contents of elements are normalized to chondrite Cl (McDonough and Sun, 1995). Eu* = $(Sm_N + Gd_N)/2$. $TE_{1,3}$, tetrad effect of fractionation of REE as mean between first and second tetrads (after (Irber, 1999). Irber, 1999).

zircon crystals (McNaughton et al., 2005; Schaltegger, 2007).

Table 1 lists representative chemical analyses of ten samples of magmatic zircon.

Magmatic zircon differs by high Hf, Y, Sc, and heavy REE concentrations. It has a high positive Ce anomaly and negative Eu anomaly. It is well known that zircon pertains to the mineral group with selective HREE (Er, Yb, Lu) concentrators, which is also confirmed by our data. In the studied zircon, the concentrations of erbium vary from 72.1 to 93.3; yttrium, from 164 to 241; and lutetium, from 32.1 to 51.3 ppm.

Table 2 lists representative analyses of hydrothermal zircon. Hydrothermal zircon differs from the magmatic variety by significantly smaller Sc and Y concentrations, but higher Nb and Ta concentrations.

Table 2. Chemical composition of hydrothermal zircon from the Elinovskii occurrence (oxides in wt %, trace elements in ppm)

Component	1	2	3	4	5	6	7	8	9
SiO_2	32.3	33.4	33.1	33.2	33.3	33.4	33.1	33.2	33.1
ZrO_2	63.8	63.3	63.5	63.4	63.2	63.3	63.7	63.5	63.7
P_2O_5	0.03	0.03	0.03	0.05	0.03	0.03	0.04	0.03	0.03
Sc	55	57	46	53	68	55	51	59	55
Ti	455	505	568	570	496	503	498	507	608
Y	52.5	47.3	43.6	33.2	41.6	43.8	42.5	41.6	42.9
Nb	32.9	32.8	33.2	33.9	52.9	43.8	44.7	53.9	92.7
La	30.5	40.1	54.9	50.6	65.1	54.7	43.1	70.7	55.2
Ce	361.2	444.1	531.1	629.3	649.1	533	426.7	538.1	533.2
Pr	65.6	53.6	63.9	102.7	83.7	49.8	90.0	82.8	51.7
Nd	121	244.1	121.1	119.0	118.0	117.3	113.1	135.8	117.8
Sm	32.04	51.63	41.95	61.57	52.09	62.04	61.6	72.1	62.11
Eu	0.63	0.70	0.69	0.87	0.81	0.55	0.8	1.13	0.87
Gd	50.1	48.3	49.1	57.1	89.1	101.1	103.5	210.1	140.4
Tb	33.2	42.6	52.7	52.6	52.9	43.1	53.3	53.6	63.2
Dy	439.7	432	336.2	322	238.4	243.6	343	444.5	343.2
Ho	115.6	212.4	213.8	212.4	214.6	217.3	127.0	317.4	216.8
Er	380.8	462.1	368.2	262.1	374.8	387.9	386.6	492.3	488.1
Tm	109.0	105.1	126.2	135.1	128.3	213.4	211.5	222.1	221.1
Yb	498	354	470	354	289	242	328	332	328
Lu	143.8	132.1	134.6	132.1	141.3	151.3	148.6	151	109.8
Hf	3894	4897	4989	4997	4994	4896	4995	4898	4896
Ta	38.8	27.2	27.8	17.2	18.7	19.6	10.3	10.5	19.5
Pb	29.0	37.9	92.7	57.9	60.6	56.6	59.2	41.6	83.4
Th	192	176	225	176	241	162	190	237	193
U	1213	1116	1515	1465	1485	1406	1454	1449	1463
ΣREE	2433.4	2670	2608	2514.3	2538.7	2466.9	2480.2	3165.2	2774.2
Th/U	0.16	0.16	0.15	0.12	0.16	0.11	0.13	0.16	0.13
$(La/Yb)_N$	0.04	0.08	0.08	0.2	0.2	0.15	0.09	0.1	0.1
Eu/Eu*	0.049	0.043	0.046	0.044	0.038	0.021	0.032	0.024	0.026
Ce/Ce*	1.33	1.84	1.79	1.47	1.71	2.16	1.13	1.4	2.09
Y/Ho	0.45	0.22	0.2	0.15	0.19	0.2	0.33	0.13	0.19
TE_3	1.76	1.48	1.44	1.31	0.89	0.76	1.3	0.66	0.93

It contains a significantly larger total REE concentration. Compared to the magmatic variety, hydrothermal zircon has an even higher negative Eu anomaly, and the positive Ce anomaly is substantially reduced. Hydrothermal zircon manifests two types of the tetrad effect of fractionation (TEF) for the third tetrad. The value of TEF of M-type REE has a narrower interval (a threshold value greater than 1.1), which varies from 1.3 to 1.76. The TEF of W-type REE (lower than the threshold level of 0.9) fluctuates from 0.89 to 0.66. The occurrence of both types of TEF of REE in hydrothermal zircon points to quite nonequilibrium conditions of zircon crystallization.

Close results on the composition of magmatic and hydrothermal zircon were obtained for the Berger massif in China (Yang et al., 2014).

DISCUSSION

It is commonly believed that hydrothermal zircon differs from high-temperature magmatic zircon in crystal morphology (Pupin, 1980; McNaughton et al.,

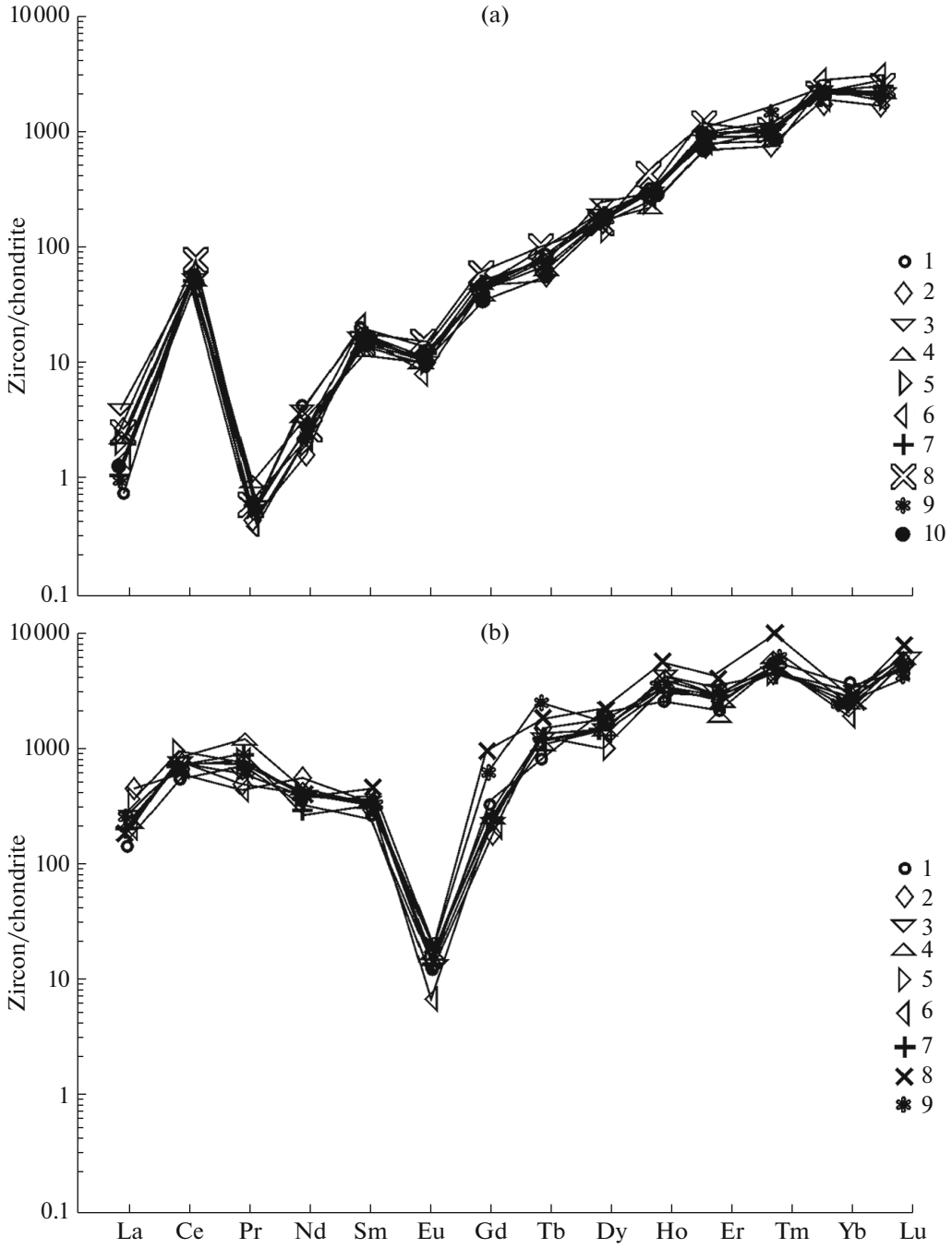

Fig. 2. REE distributions in magmatic (a) and hydrothermal (b) zircon normalized with respect to Cl chondrite (McDonough and Sun, 1995). Sample numbers correspond to those in Table 1.

2005) and chemical composition ((Hoskin, Schaltegger, 2003; Hoskin, 2005), including chondrite-normalized REE distributions, Th/U ratio, and degree of radiogenic Pb loss (Hoskin and Schaltegger, 2003; Hoskin, 2005; Pettke et al., 2005; Geisler et al., 2007; Harley and Kelly, 2007; Schaltegger, 2007).

The REE distribution spectra for magmatic zircon have a starkly pronounced differentiated character of the REE distribution with a positive Ce anomaly and negative Eu anomaly (Fig. 2), which is weakly expressed (Eu/Eu* varies from 0.3 to 0.52).

The composition of magmatic zircon of the Elinovskii massif is characterized by a stochiometric Zr and Si ratio, whereas hydrothermal zircon is depleted in Zr. The REE distribution spectra in hydrothermal zircon differ sharply from those in the magmatic variety (Fig. 2). The spectrum has a jagged character. The negative Eu anomaly is distinctly expressed (Eu/Eu*

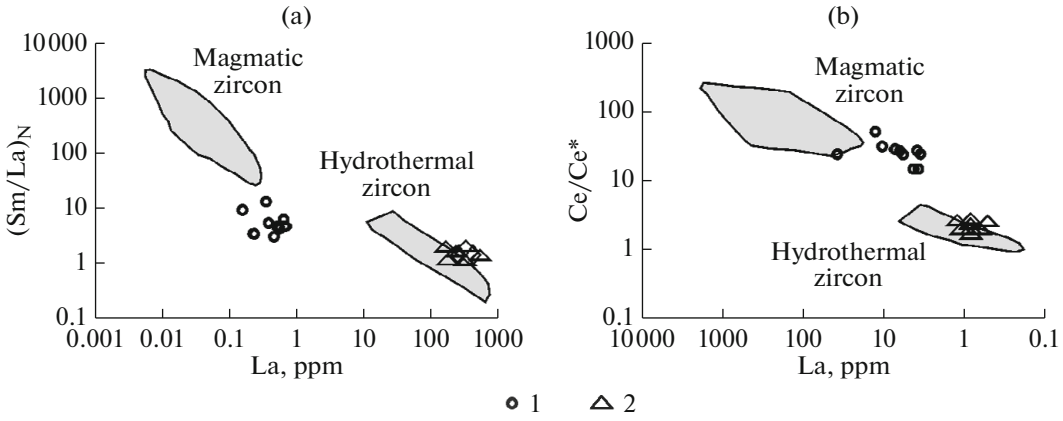

Fig. 3. Discriminant diagrams of (a) (Sm/La)N vs. La (ppm), (b) Ce/Ce* vs. (Sm/La)N (Hoskin, 2005). Plots include data for magmatic zircon (1) and hydrothermal zircon (2) from the Elinovskii massif.

varies from 0.024 to 0.049). In addition, in hydrothermal zircon, such impurity elements as U, Th, Nb, Ta, Pb, Ti, and LREE have higher concentrations than in magmatic zircon. This is probably because elements with large ionic radii are incompatible with the structure of magmatic zircon (Hanchar and Westrenen, 2007) but compatible in magmatic fluids (Bakker and Elburg, 2006). High LREE and Ti concentrations in hydrothermal zircon may result from the presence of submicroscopic and even nanoscale inclusions (Geisler et al., 2007).

An alternative explanation for the increased LREE and Ti concentrations in hydrothermal zircon may be the behavior of elements that are not regulated by charge and radius (Bau and Dulski, 1995). A similar behavior of elements is frequently encountered in highly evolved melt systems enriched in H_2O, CO_2, and volatiles, such as Li, B, F, and/or Cl, at the transition stage from silicate melt to aqueous fluids (Veksler, 2004).

It is well known that the non-charge- and non-radius-controlled behavior of elements is frequently accompanied by the TEF of REE. It is noteworthy that both of the indicated peculiarities are observed in zircon from highly differentiated granite magmas that underwent intensive hydrothermal or autopneumatic-lithic alteration (Masuda and Ikeuchi 1979; Bau, 1999; Irber, 1999; Veksler et al., 2005).

Imaging points for the compositions of the studied zircon in the $(Sm/La)_N$–La discriminant diagram of (Hoskin, 2005) are distinctly combined in two clusters: magmatic zircon plots in the magmatic field, while hydrothermal zircon plots in the hydrothermal field (Fig. 3a). A similar pattern is observed in the $(Sm/La)_N$–Ce/Ce* diagram (Fig. 3b). It is noteworthy that in both groups of zircon, a positive Ce anomaly is observed (particularly strong for magmatic zircon, with values from 28.3 to 87.9, and weaker in the case of hydrothermal zircon, from 1.2 to 2.3), as well as a negative Eu anomaly. The lack of points for the studied zircon in the magmatic field in the diagrams is probably due to reworking of rocks and minerals by magmatic fluid in nonequilibrium conditions (Hoskin, 2005; Skublov et al., 2013).

In the Yb–U, Hf–U/Yb, Y–U/Yb discriminant diagrams, comparable zircon groups plot in the continental zircon field (Grimes et al., 2007) or tend toward it (Fig. 4a–4c). Lowered Y concentrations (Fig. 4c) in hydrothermal zircon is likely related to the presence of fluorite and xenotime in ores, which concentrate the majority of yttrium. Since zircon in hydrothermal paragenesis is associated with monazite, xenotime, and synchysite, decreased concentrations of Hf are likely, because these minerals also accumulate this element.

Because the composition of zircon manifests a positive Ce anomaly, the TEF of REE for hydrothermal zircon was computed for the third tetrad and an Eu/Eu*–TE_3 diagram was constructed (Fig. 5). From the diagram it is clear that all the values for the Eu/Eu* ratio are lower than the same value in chondrite; here, two clusters of imaging points and two opposing trends are distinguished: one for the significant TEF of M-type REE values and the other for the TEF of W-type REE. As well, a correlation of the trends of the TEF REE values for both types with the Eu/Eu* ratio is observed. An increase in the M-type REE TEF correlates with an increase in the Eu/Eu* ratio, whereas a decrease in the W-type REE TEF correlates with a weak decrease in the Eu/Eu* anomaly. This can be explained by the quite variable physicochemical conditions of the hydrothermal process during which zircon crystallized. An increase in the Eu/Eu* value with manifestation of M-type REE TEF in accordance with the series of acidity/alkalinity of the elements (Marakushev, 1976) of the spectrum of Sm, Gd, Eu in aqueous–sulfurous solutions corresponds to an increase in the acidity of the medium, whereas a decrease in the Eu/Eu* values with manifestation of W-type REE TEF corresponds to an increase in the

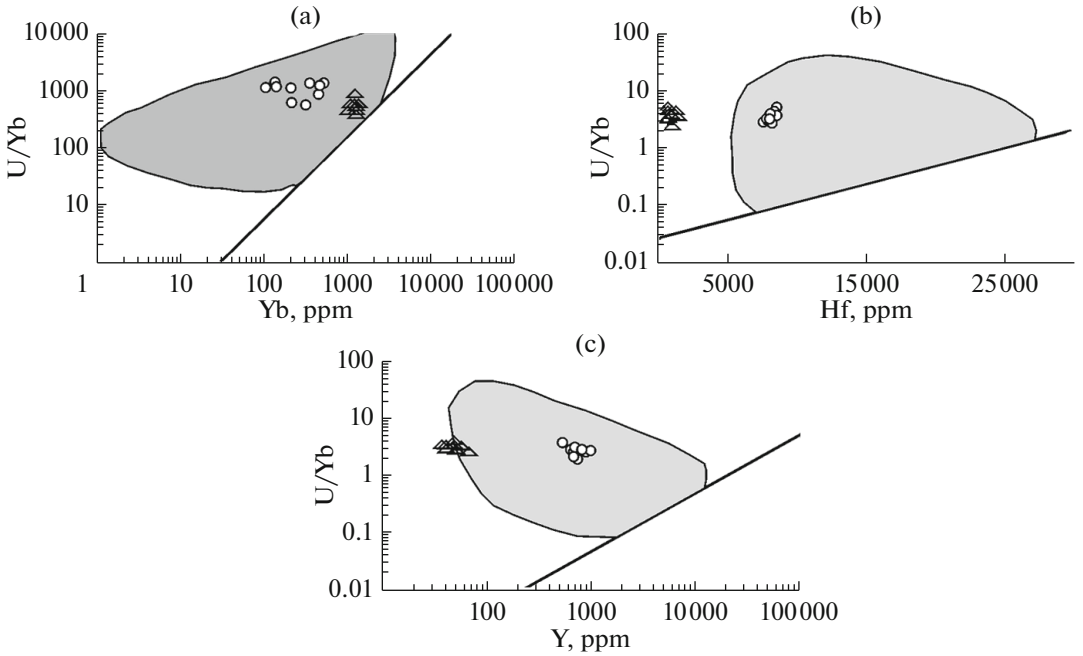

Fig. 4. Discriminant diagrams of (a) U/Y vs. Yb, (G) U/Yb vs. Hf , (в) U/Yb vs. Y. Shaded field represents the compositional range of continental crust zircon, solid line on each diagram indicates upper limit for zircon that is oceanic-crustal in origin (after Grimes et al., 2007). Symbols are same as in Fig. 3.

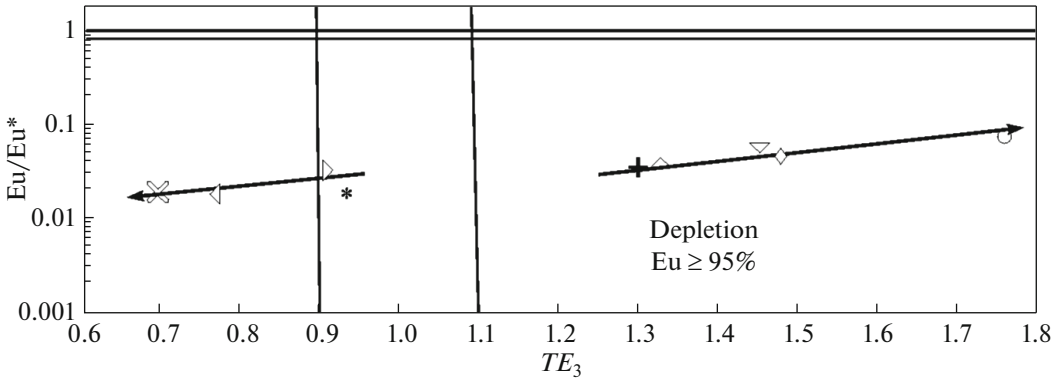

Fig. 5. Tetrad effect (TE_3) vs. Eu/Eu* for hydrothermal zircon. Symbols are same as in Fig. 2 for hydrothermal zircon.

alkalinity of the medium. We observed similar regularities for strongly evolved anorogenic granitoids (Gusev and Tabakaeva, 2015).

CONCLUSIONS

Magmatic and hydrothermal zircon differ in their morphological features and chemical compositions. These differences are caused not only by the crystallization temperatures, but also by the peculiarities of the fluid regime and the composition of magmatic volatiles. Hydrothermal zircon is characterized by a noncharge- and non-radius-controlled behavior of REE, related to the high degree of differentiation of granitic melts enriched in H_2O, CO_2, and such volatile components as Li, B, F, and/or Cl. Zircon manifests a tetrad effect of fractionation of M-type REE. The studied zircon of the Elinovskii magma–ore–metasomatic system demonstrates the peculiarities of the REE composition typical of zircon from continental rocks.

REFERENCES

Aja, S.U., Wood, S.A., and Williams, JonesA.E., *The solubility of some alkali-bearing Zr minerals in hydrothermal solu-*

tions, Aqueous Chem. Geochem. Oxides, Oxyhydroxides, Relat. Mater., 1997, vol. 432, pp. 69–74.

Avers, J., Zhang, L., Luo, Y., and Peters, T., Zircon solubility in alkaline aqueous fluids at upper crustal conditions, *Geochim. Cosmochim. Acta*, 2012, vol. 96, pp. 18–28.

Bakker, R.J. and Elburg, M.A., A magmatic-hydrothermal transition in Arkaroola (northern Flinders Ranges, South Australia): from diopside–titanite pegmatites to hematite-quartz growth, *Contrib. Mineral. Petrol.,* 2006, vol. 152, pp. 541–569.

Bau, M., Scavenging of dissolved yttrium and rare earths by precipitating iron oxyhydroxide: experimental evidence for Ce oxidation, Y–Ho fractionation, and lanthanide tetrad effect, *Geochim. Cosmochim. Acta,* 1999, vol. 63, pp. 67–77.

Bau, M. and Dulski, P., Comparative-study of yttrium and rare-earth element behaviors in fluorine-rich hydrothermal fluids, *Contrib. Mineral. Petrol.,* 1995, vol. 119, pp. 213–223.

Belousova, E.A., Griffin, W.L., and O'Reilly, S.Y., Zircon crystal morphology, trace element signatures and Hf isotope composition as a tool for petrogenetic modelling: examples from Eastern Australian granitoids, *J. Petrol*, 2006, vol. 47, pp. 329–353.

Finlowbates, T. and Stumpfl, E.F., The behavior of so-called immobile elements in hydrothermally altered rocks associated with volcanogenic submarine-exhalative ore deposits, *Miner. Deposita,* 1981, vol. 16, pp. 319–328.

Fu, B., Mernagh, T.P., Kita, N.T., Kemp, A.I.S., and Valley, J.W., Distinguishing magmatic zircon from hydrothermal zircon: a case study from the Gidginbung high-sulphidation Au–Ag–(Cu) deposit, SE Australia, *Chem. Geol.,* 2009, vol. 259, pp. 131–142.

Gasquet, D., Pelleter, E., Cheilletz, A., Mouttaqi, A., Annich, M., El Hakour, A., Deloule, E., and Feraud, G., Hydrothermal zircons: a tool for ion microprobe U–Pb dating of gold mineralization (Tamlalt-Menhou-hou gold deposit Morocco), *Chem. Geol.,* 2007, vol. 245, pp. 135–161.

Gusev, A.I. and Tabakaeva, E.M., *Petrology, Geochemistry and Genesis of Anorogenic Granitoids,* Hamburg: Palmarium Academic Publishing, 2015.

Hanchar, J.M. and Westrenen, W.V., Rare earth element behavior in zircon–melt systems, *Elements,* 2007, vol. 3, pp. 37–42.

Harley, S.L. and Kelly, N.M., Zircon tiny but timely, *Elements*, 2007, vol. 3, pp. 13–18.

Hoskin, P.W.O. and Schaltegger, U., The composition of zircon and igneous and metamorphic petrogenesis, *Rev. Mineral. Geochem.*, 2003, vol. 53, pp. 21–62.

Hoskin, P.W.O., Trace-element composition of hydrothermal zircon and the alteration of Hadean zircon from the Jack Hills, Australia, *Geochim. Cosmochim. Acta,* 2005, vol. 69, pp. 637–648.

Irber, W., The lanthanide tetrad effect and its correlation with K/Rb, Eu/Eu*, Sr/Eu, Y/Ho, and Zr/Hf of evolving peraluminous granite suites, *Geochim. Comochim. Acta,* 1999, vol. 63, pp. 489–508.

John, B.-M., Wu, F.Y., Capdevila, R., Martineau, F., Zhao, Z.H., and Wang, Y.X., Highly evolved juvenile granites with tetrad REE patterns: the Woduhe and Baerzhe granites from the Great Xing'an Mountains in NE China, *Lithos,* 2001, vol. 59, pp. 171–198.

Lawrie, K.C., Mernagh, T.P., Ryan S.G., van Achterbergh, E., and Black, L.P., Chemical fingerprinting of hydrothermal zircons: an example from the Gidginbung high sulphidation Au–Ag–(Cu) deposit, New South Wales, Australia, *Proc. Geol. Assoc.,* 2007, vol. 118, pp. 37–46.

Van Lichtervelde, M., Melcher, F., and Wirth, R., Magmatic vs. hydrothermal origins for zircon associated with tantalum mineralization in the Tanco pegmatite, Manitoba, Canada, *Am. Mineral.,* 2009, vol. 94, pp. 439–450.

Van Lichtervelde, M., Holtz, F., and Hanchar, J.M., Solubility of manganotantalite, zircon and hafnon in highly fluxed peralkaline to peraluminous pegmatitic melts, *Contrib. Mineral. Petrol.,* 2010, vol. 160, pp. 17–32.

Marakushev, A.A., *Thermodynamic factors of ore zoning formation, Prognozirovanie skrytogo orudeneniya ba osnove zonal'nosti gidrotermal'nykh mestorozhdenii* (Prediction of Hidden Mineralization on the Basis of Zoning of Hydrothermal Deposits), Moscow: Nauka. 1976. P. 36-51 (in Russian).

Masuda, A. and Ikeuchi, Y., *Lanthanide tetrad effect observed in marine environment. Geochem. J.,* 1979, vol. 13, pp. 19–22.

Mazdab, F., Wooden, J.L., Cheadle, M.J., Hanghoj, K., and Schwartz, J.J., The trace element chemistry of zircons from oceanic crust: a method for distinguishing detrital zircon provenance, *Geology,* 2007, vol. 35, pp. 643–646.

McDonough, W.F. and Sun, S., The composition of the Earth, *Chem. Geol,* 1995, vol. 120, pp. 223– 253.

McNaughton, N.J., Mueller, A.G., and Groves, D.I., The age of the giant Golden Mile deposit, Kalgoor-lie, Western Australia: ion-microprobe zircon and monazite U-Pb geochronology of a synmineralization lamprophyre dike, *Econ. Geol.,* 2005, vol. 100, pp. 1427–1440.

Skublov, S.G., Myskova, T.A. and Marin, Yu.B., Astaf'ev, B.Yu., Bogomolov, E.S., and L'vov, P.A., Geochemistry of zircon rims with different ages in gneisses of the Kola Series (SIMS, SHRIMP-II) and the problem of early Caledonian thermal activization of the Kola craton. *Dokl. Earth Sci.,* 2013, vol. 453, pp. 1250–1256.

Pettke, T., Audetat, A., Schaltegger, U., and Heinrich, S.A., Magmatic-to hydrothermal crystallization in the W–Sn mineralized Mole granite (NSW, Australia)—Part II: evolving zircon and thorite trace element chemistry, *Chem. Geol.,* 2005, vol. 220, pp. 191–213.

Pupin, J.P. and Turco, G., *Unetypologie originale du zircon accessoire, Bull. Soc. Franc. Mineral. Cristallogr.*, 1972, vol. 95, pp. 348–359.

Pupin, J.P., Zircon and granite petrology, *Contrib. Mineral. Petrol.,* 1980, vol. 73, pp. 207–220.

Rubin, J.N., Henry S.D., and Price J.G., Hydrothermal zircons and zircon over growths, Sierra-Blanca peaks, Texas, *Am. Mineral.,* 1989, vol. 74, pp. 865–869.

Salvi, S. and Williams-Jones, A.E., Alteration, HFSE mineralization and hydrocarbon formation in pe-ralkaline igneous systems: insights from the Strange Lake Pluton, Canada, *Lithos,* 2006, vol. 91, pp. 19–34.

Schaltegger, U., Hydrothermal zircon. *Elements,* 2007, vol. 3, pp. 51–68.

Schaltegger, U. and Tomaschek, F., Re-equilibration of zircon in aqueous fluids and melts, *Elements,* 2007, vol. 3, pp. 43–50.

Schaltegger, U., Pettke, T., Audetat, A., Reusser, E., and Heinrich, S.A., Magmatic-to-hydrothermal crystallization in the W–Sn mineralized mole granite (NSW, Australia). part I: crystallization of zircon and REE phosphates over three million years—a geochemical and U–Pb geochronological study, *Chem. Geol.,* 2005, vol. 220, pp. 215–235.

Valley, P.M., Hanchar, J.M., and Whitehonse, M.J., Direct dating of Fe oxide–(Cu–Au) mineralization by U/Pb zircon geochronology, *Geology,* 2009, vol. 37, pp. 223–226.

Valley, P.M., Fisher, S.M., Hanchar, J.M., Lam, R., Tubrett, M., Hafnium isotopes in zircon: a tracer of fluid-rock interaction during magnetite-apatite ("Kiruna-type") mineralization, *Chem. Geol.,* 2010, vol. 275, pp. 208–220.

Veksler, I.V., Liquid immiscibility and its role at the magmatic hydrothermal transition: a summary of experimental studies, *Chem. Geol.,* 2004, vol. 210, pp. 7–31.

Veksler, I.V., Dorfman, A.M., Kamenetsky, M., Dulski, P., and Dingwell, D.B., Partitioning of lanthanides and Y between immiscible silicate and fluoride melts, fluorite and cryolite and the origin of the lanthanide tetrad effect in igneous rocks, *Geochim. Cosmochim. Acta,* 2005, vol. 69, pp. 2847– 2860.

Wayne, D.M. and Hewitt, D.A., The hydrothermal stability of zircon: preliminary experimental and isotopic studies, *Geochim. Cosmochim. Acta,* 1992, vol. 56, pp. 3551–3560.

Yang, W.-B., Niu, H.-C., Shan, O., Sun, W.-D., Zhang, H., Li, N.-B., Jiang, Yu.-H., and Yu, X.-Y., Geochemistry of magmatic and hydrothermal zircon from the highly evolved Baerzhe alkaline granite: implications for Zr–REE–Nb mineralization, *Miner. Deposita,* 2014, vol. 49., no. 4, 451–470.

Translated by A. Carpenter